Extracellular vesicles in ALS patients' cells: Characterization and study of their modulation upon pharmacological treatment

Jesús Alejandro Bueso de Barrio

Nanobiotechnology, June 2022

Master's thesis

Materials and Production
Aalborg University
https://www.mp.aau.dk

AALBORG UNIVERSITY
STUDENT REPORT

Title:
Extracellular vesicles in ALS patients' cells: Characterization and study of their modulation upon pharmacological treatment.

Project:
Master's thesis

Project Period:
September 2021 - June 2022

Participant:
Jesús Alejandro Bueso de Barrio

Supervisors:
Valle Palomo
Peter Fojan

Page Numbers: 43

Date of Completion:
June 1, 2022

Abstract:

Amyotrophic lateral sclerosis (ALS) is a neurodegenerative disease which affects the lower and upper motor neurons, which are responsible for voluntary movements. The causes of the disease are unknown, and the disease remains incurable. Due to its heterogeneity, drug development for ALS comprises a great challenge.
Cell models obtained from patients' blood have been used for the experimental procedures carried out on this project. These models recapitulate the TAR-DNA binding protein 43 (TDP-43) abnormalities observed in patient neurons.
For this project, the size, concentration and ALS related biomolecules content of extracellular vesicles (EVs) produced by lymphoblastic ALS models and control lymphoblasts have been studied. EVs have been labelled with Quantum Dot nanoparticles (QD). The effects of a casein kinase 1δ (CK-1δ) inhibitor on these EVs have been analyzed.

Abbreviation list

AD Alzheimer's disease

AFM Atomic force microscopy

ALS Amyotrophic lateral sclerosis

C9orf72 Chromosome 9 open reading frame 72

CK-1δ Casein kinase 1δ

CNS Central nervous system

CSF Cerebrospinal fluid

DMSO Dimethyl sulfoxide

DNA Deoxyribonucleic acid

EAAT1 Excitatory amino acid transporter 1

EMA European Medicines Agency

ER Endoplasmic reticulum

EVs Extracellular vesicles

FALS Familial amyotrophic lateral sclerosis

FDA U.S. Food and Drug Administration

FRET Förster or fluorescence resonance energy transfer

FTD Frontotemporal dementia

L1CAM L1 cell adhesion molecule

MND Motor neuron disease

NES Nuclear export signal

NLS Nuclear localization signal

NTA Nanoparticle tracking analysis

PBMCs Peripheral blood mononuclear cells

PCR Polymerase chain reaction

QD Quantum Dot nanoparticles

RNA Ribonucleic acid

RNP Ribonucleoprotein

ROS Reactive oxygen species

SALS Sporadic amyotrophic lateral sclerosis

SEM Standard error of the mean

TDP-43 TAR-DNA binding protein 43

TEM Transmission electron microscopy

Tb Terbium

crRNA Crispr ribonucleic acid

iPSC Induced pluripotent stem cells

lncRNA Long non-coding ribonucleic acid

mRNA Messenger ribonucleic acid

miRNA Micro ribonucleic acid

qPCR Quantitative polymerase chain reaction

Contents

1 Introduction

1.1 Amyotrophic Lateral Sclerosis

ALS is a neurodegenerative disease which affects the lower motor neurons (neurons that project from the brain stem or spinal cord to muscle) and upper motor neurons (neurons that project from the cortex to the brain stem and the spinal cord). The degeneration of both upper and lower motor neurons leads to muscle weakness, twitching and cramping; stiffness, and hyperreflexia. Ultimately, patients die within 2-5 years from diagnosis [1–3].

The causes of ALS are unknown, and the disease remains incurable. Nevertheless, significant advances have been made in the understanding of both, the genetic and environmental components of the disease [4].

1.1.1 Epidemiology

With an incidence between 0.6 and 3.8 per 100,000 person per year, it is the most prevalent motor neuron disease (MND). However, due to the fast progression of the disease, about 50% of patients die within 2 years from diagnosis, resulting in a low prevalence (between 4.1 and 8.4 per 100,000 persons) and is thus classified as a rare disease [2, 5].

1.1.2 Treatment

There are currently two drugs approved by the U.S. Food and Drug Administration (FDA) for the treatment of ALS, edaravone and riluzole. The latter one has also been approved by the European Medicines Agency (EMA). However, these drugs provide modest benefits in life expectancy and there is a need for a treatment which modifies the disease [6, 7].

1.1.3 Amyotrophic Lateral Sclerosis and Frontotemporal Dementia

Frontotemporal dementia (FTD) is a heterogeneous group of clinical syndromes marked by the progressive, focal neurodegeneration of the frontal and anterior temporal lobes

[8]. It is one of the most common types of dementia in people under 65, and it is often underdiagnosed, as symptoms overlap with psychiatric manifestations [8, 9]. The clinical presentations include behavioral changes and deficits in language and other cognitive functions [10]. Genetic studies of the disorder have led to the conclusion that FTD and ALS have a significant genetic overlap; *TARDBP*, *SQSTM1*, *VCP*, *FUS*, *TBK1*, *CHCHD10*, and especially chromosome 9 open reading frame 72 (*C9orf72*), are the critical genetic players in these neurological disorders [11]. Similarly to ALS, there is no effective treatment which prevents, cures or slows the progression of FTD [8].

1.1.4 Etiology

Most ALS cases are considered sporadic amyotrophic lateral sclerosis (SALS), meaning that there is no obvious genetically inherited component, with only 5 to 10% of the cases being genetic; namely, familial amyotrophic lateral sclerosis (FALS) [2, 3]. The responsible genes that have been identified for ALS can be seen in Table 1.1.

Table 1.1: **Monogenic causes of amyotrophic lateral sclerosis (ALS).** Abbreviations: AD autosomal-dominant, AR autosomal-recessive, DN *de novo*, XL X-linked, NA not available, GEF guanine nucleotide exchange factor, ER-UPR, endoplasmic reticulum unfolded protein response, PtdIns(3,5)P2 phosphatidylinositol 3,5-bisphosphate, EGF epidermal growth factor, EGFR EGF receptor. Adapted from Volk et al. [12], Benarroch et al. [13].

Gene	Inheritance	Function / Proposed function	Gene	Inheritance	Function / Proposed function
C9orf72	AD, DN	Autophagy-lysosome pathway	*CCNF*	AD	Centrosomal duplication
FUS	AD, DN	DNA/RNA related processes and regulation	*TARDBP/ TDP43*	AD	DNA/RNA related processes and regulation
SOD1	AD, AR, DN	Removal of superoxide radicals	*NEK1*	AD	DNA damage checkpoint control and repair
TBK1	AD, DN	Inflammatory responses to foreign agents	*VCP*	AD, DN	Membranes fragmentation and reassembly
SQSTM1	AD	Selective macroautophagy	*KIF5A*	AD	Axonal transport
CHCHD10	AD	Mitochondrial organization and structure	*PFN1*	AD	Actin binding, affects cytoskeleton structure
SIGMAR1	AR	Lipid transport, neurotransmitter release, calcium signaling, EGF signaling	*ALS2*	AR	GTPase regulator, survival and growth of spinal motoneurons
NEFH	AD, AR	Maintenance of neuronal caliber	*ANXA11*	AD	Midbody formation, cytokinesis
HNRNPA1	AD, DN	pre-mRNA packaging, poly(a) transport, splice site selection	*HNRNPA2B1*	AD	pre-mRNA packaging, telomeric DNA protection
CHMP2B	AD	Multivesicular bodies formation	*SPG11*	AR	Neurite plasticity
SETX	AD	RNA metabolism and genomic integrity	*FIG4*	AD	Synthesis and turnover of PtdIns(3,5)P2

continued on next page

Table 1.1 continued from previous page

Gene	Inheritance	Function / Proposed function	Gene	Inheritance	Function / Proposed function
ALS3	AD	NA	*ALS7*	AD	NA
VAPB	AD	ER-UPR	*ANG*	AD	RNA regulation
UBQLN2	XL	Protein degradation	*ATXN2*	AD	EGFR trafficking
TUBB4A	AD	Major constituent of microtubules	*DCTN1*	AD	Dynein-mediated retrograde transport, microtubule stability
TUBA4A	AD	Major constituent of microtubules	*MATR3*	AD	Transcription and RNA regulation
OPTN	AD, AR	Maintenance of Golgi complex, membrane trafficking, exocytosis	*ERBB4*	AD	Receptor for neuregulins and EGF, development of the heart, CNS, cellular proliferation, differentiation, apoptosis

The prevalence and the proportion of causative genes in FALS and SALS is shown in Figure 1.1. The repeated hexanucleotide expansion mutation (GGGGCC) in *C9orf72* gene is the most prevalent mutation in ALS. Usually, individuals carry 2 to 10 hexanucleotide GGGGCC repeats in the *C9orf72* gene, while more than a few hundred repeats represent a risk not only for ALS but also for FTD. Additionally, patients with *C9orf72*-related ALS/FTD usually have TDP-43 cytoplasmic inclusions at post-mortem analysis [14–16].

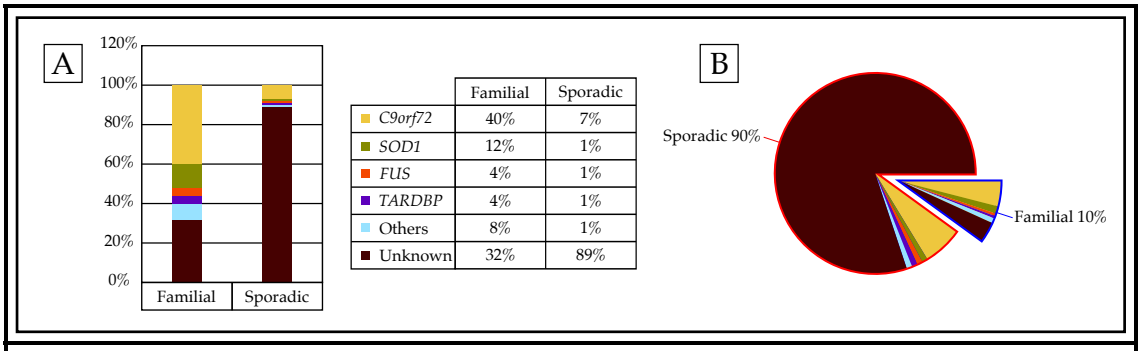

	Familial	Sporadic
C9orf72	40%	7%
SOD1	12%	1%
FUS	4%	1%
TARDBP	4%	1%
Others	8%	1%
Unknown	32%	89%

Figure 1.1: **A) Proportion of causative genes in familial and sporadic ALS. B) Visual representation of causative genes by prevalence of FALS and SALS.** The majority of cases are sporadic (90%).
Adapted from Yun and Ha [17].

Mutations in the *SOD1* gene also have a great impact on FALS. SOD1 is a powerful antioxidant enzyme that protects cells from the damaging effects of superoxide radicals by reducing them into hydrogen peroxide and diatomic oxygen. Mutated *SOD1* gene can result in either gain or loss of function mutations. Loss of function SOD1 mutations results in insufficient degradation of reactive oxygen species (ROS), damaging the substrates required by motor neurons. Gain of function SOD1 mutations may cause an increase in oxidative activity resulting in excessive production of hydrogen peroxide radicals and increased protein-protein interactions. Interestingly, the oxidation of both, the mutated and the wild type SOD1 protein by hydrogen peroxide is a phenomenon that may promote its aggregation, acquiring toxic properties [18, 19].

1.1.5 TDP-43 proteinopathy

Encoded by *TARDBP* gene, TDP-43 is a ubiquitously expressed DNA/RNA-binding protein. It contains two RNA recognition motifs, RRM1 and RRM2, a nuclear localization signal (NLS), a nuclear export signal (NES) and a glycine-rich C-terminus that mediates protein–protein interactions, as well as five putative mitochondria localization signals. Oxidation of the RNA recognition motifs induces the aggregation of the protein [20–22].

TDP-43 is predominantly localized in the nucleus, however, it can shuttle to and from the cytoplasm. The functions of TDP-43 are represented in Figure 1.2. In the nucleus, TDP-43 functions are related to messenger ribonucleic acid (mRNA) processes, such as splicing, RNA stabilization, transcriptional and translational regulation, micro ribonucleic acid (miRNA) and long non-coding ribonucleic acid (lncRNA) processing. In the cytoplasm, TDP-43 participates in stress granules formation; membrane-less organelles that assemble in response to environmental stressors, such as oxidative stress, heat shock and osmotic stress. They disassemble upon stress cessation [23–25].

Even though TDP-43 is mainly a nuclear protein, it can be shuttled to the cytoplasm, and thus it has been shown that TDP-43 exists in the endoplasmic reticulum (ER), mitochondria and their associated membranes, RNA granules, and stress granules to regulate the ER-mitochondria binding, mitochondrial protein translation, and mRNA transport and translation [25, 26].

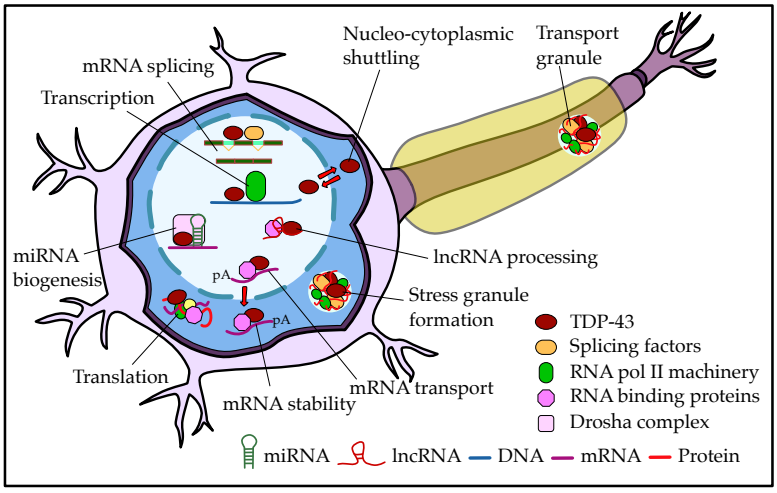

Figure 1.2: **TDP-43 functions.** TDP-43 is involved in diverse functions in the nucleus associated to mRNA, such as splicing, RNA stability, miRNA and lncRNA processing. It is predominantly a nuclear protein but it can be shuttled to the cytoplasm, where it is involved in the stress granules formation, ribonucleoprotein transporting granules formation, translation and other processes.
Abbreviations: lncRNA long non-coding RNA, miRNA microRNA, mRNA messenger RNA, pA poly(A) tail.
Adapted from de Boer et al. [27].

The majority of SALS patients (up to 97%) contain TDP-43 protein deposited in neuronal inclusions [23, 28]. TDP-43 proteinopathies are characterized by nuclear-to-cytoplasmic mislocalization, aberrant phosphorylation, ubiquitination, deposition of ubiquitinated and hyper-phosphorylated TDP-43 into inclusion bodies, protein truncation leading to formation of toxic C-terminal TDP-43 fragments, and protein aggregation [23]. TDP-43 proteinopathy is a common prominent pathological feature of various major neurodegenerative diseases including ALS, FTD, and Alzheimer's disease (AD) [29]. Increasing evidence suggests that nuclear-to-cytoplasmic mislocalization of TDP-43 induces toxicity through both loss and gain of function mechanisms [25].

The gain of function refers to the cytotoxicity of hyperphosphorylated and aggregated TDP-43 under abnormal conditions. For example, TDP-43 phosphorylation and ubiquitination are the main pathological changes in patients with TDP-43 proteinopathy, which increase the formation of insoluble inclusions, interfere with the normal function of TDP-43 and lead to a cytotoxic form of TDP-43. In addition, as the C-terminal fragment of TDP-43 has a similar sequence to prion proteins, the spread of this toxic peptide in adjacent neurons may also be pathogenic. On the other hand, loss of function refers to the weakening or disappearance of normal functions of nuclear TDP-43 after structural change, resulting in abnormal neuronal function including impaired protein degradation, changes in TDP-43-related splicing events, nuclear transport defects, loss of TDP-43 automatic adjustment, and the enhancement of TDP-43 self-interaction promoting aggregation [26].

1.1.6 TDP-43 cell-to-cell propagation

In vitro studies have demonstrated that both wild-type and disease mutant TDP-43 and its C-terminal fragments can oligomerise and form amyloid like fibrils which can exhibit

prion-like infectious seeding ability to cells expressing the soluble TDP-43 [30, 31].

Cellular studies have suggested that TDP-43, including oligomeric forms, can be transmitted between cells, spreading the pathology among them. The presence of pathological proteins in the EVs has led to the hypothesis that the transmission may occur via EVs secretion [30, 32].

EVs are a heterogeneous population of naturally occurring nano to micro-sized membrane vesicles [33]. They can be classified and differentiated based on size, biogenesis and release pathways. The most researched EVs are exosomes and ectosomes (also referred to as microvesicles) which play key roles in intercellular communication [34, 35]. The term exosome refers to 30-120 nm diameter vesicles released upon multivesicular endosome fusion with the plasma membrane; the exosome precursors (intraluminal vesicles) originate from the membrane of endocytic cisternae by inward budding of microdomains, and they eventually become multivesicular endosomes upon accumulation [34–36]. On the other hand, ectosomes bud directly from the plasma membrane and are normally bigger (up to 1000 nm in diameter) [34, 36]. The differences between exosomes and ectosomes can be seen in Figure 1.3.

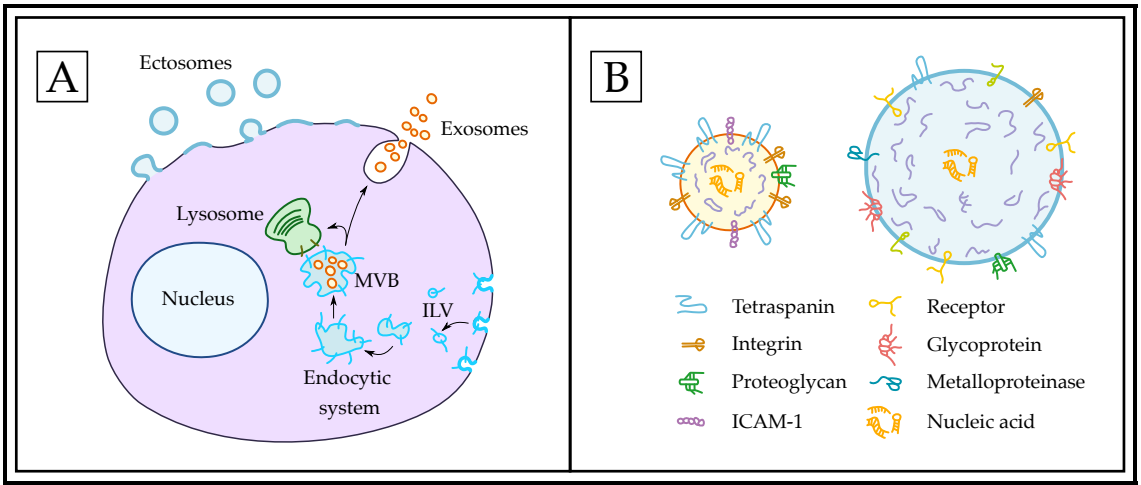

Figure 1.3: **A) Generation and release of exosomes and ectosomes.** Intraluminal vesicles originate from the membrane of endocytic cisternae by inward budding of microdomains. Upon their accumulation, the cisternae become multivesicular bodies. After persisting in the cytosol for variable periods of time, some multivesicular bodies undergo exocytic fusion with the plasma membrane, releasing the exosomes. Ectosomes are formed by outward budding in the plasma membrane; once the vesicle has fissioned, it is rapidly released into the extracellular space. **B) Structure and composition of exosomes and ectosomes.** During EVs formation, tetraspanins have been reported to interact with cytosolic proteins and possibly participate in the process of luminal cargo loading. Additional tetraspanins appear to play a role in the trapping of surface and intracellular signaling proteins. Apart from tetraspanins, exosomes membranes also include flotillin, PGRL (CD81 regulatory-like protein), stomatin, L1CAM, LAMP2, integrins, the enzyme alanyl aminopeptidase N, and insoluble fibronectin. In addition to integrins, ectosomes membranes contain matrix metalloproteinase MT1-MMP, glycoprotein receptors, the adhesion protein P-selectin, and the integrin Mac-1.
Abbreviations: MVB multivesicular bodies, ILV intraluminal vesicles.
Adapted from Meldolesi [34].

Similarly to healthy cells, apoptotic cells can also release EVs. They are generally de-

scribed as vesicles with a size of up to 5 µm in diameter that carry nuclear fragments and cellular organelles such as mitochondria and endoplasmic reticulum as a result of cell apoptosis [37].

Most, if not all, cell types release EVs that then enter almost all bodily fluids [38]. EVs are highly stable and have been found in almost every human body fluid, including urine, blood, saliva, cerebrospinal fluid (CSF), synovial fluid, semen, breast milk, amniotic fluid, lymph, and bronchoalveolar lavage fluid [39, 40]. The presence of EVs in bodily fluids such as blood provides a biomarker source, which is especially interesting to study the central nervous system (CNS) and its related diseases since the samples are obtained in a non-invasive, widely available, and inexpensive method.

The isolation of neural enriched EVs is possible due to the presence of neural proteins such as L1 cell adhesion molecule (L1CAM) or excitatory amino acid transporter 1 (EAAT1) in these EVs. L1CAM is a transmembrane protein that mediates cell-to-cell adhesion at the cell nerve surface. EAAT1 and 2 are predominantly expressed in astrocytes, although they are also expressed in other types of glial cells [41]. The studies conducted by Kapogiannis' group show that L1CAM+ EVs have higher concentration of several markers that are reasonably specific to neurons (p-tau, neuron-specific enolase, MAP2, NCAM, NFL) when compared to total plasma EVs, which suggests a neuronal origin [42].

Several studies have recently obtained enriched fractions of EVs from ALS patients. A summary of these studies can be seen in Table 1.2. In these studies, there are mainly two methodologies of isolating an EVs enriched solution; namely, using a vesicle precipitating agent (e.g. ExoQuick) or by differential (ultra)-centrifugation. Once the enriched fraction has been achieved, the presence of EVs can be confirmed through different analyses, such as ELISA, western blot, transmission electron microscopy (TEM) or nanoparticle tracking analysis (NTA).

Some tetraspanins with wide cellular expression (CD9, CD63 and CD81) are highly enriched in exosomes relative to their content in the respective producing cells and have been considered as good general exosomal markers. However, these proteins are also abundantly expressed on the cell surface and thus become incorporated in other types of EVs without the need of an endocytic origin. Different reports have shown that CD9, CD63 and CD81 are not only abundant in exosomes but also in ectosomes, complicating the discrimination between these different types of EVs. The lack of specific protein markers to distinguish exosomes from ectosomes difficults the separation of exosomes from ectosomes of the same size. The study by Mathieu et al. [43] proposed that EVs bearing only CD9 or CD81 but not CD63 probably did not form in endosomes (and were thus ectosomes) due to the steady-state accumulation of CD63 in multivesicular bodies, whereas those bearing CD63 together with one or the two other tetraspanins may correspond to endosome-derived exosomes. In their work, Mathieu et al. [43] provide

evidence that small EVs bearing tetraspanins, especially CD9 and CD81 with little CD63, bud mainly from the plasma membrane, whereas others bearing CD63 with little CD9 but containing some late endosome proteins form in internal compartments and qualify as exosomes [33, 43]. However, several reports indicate that the differences between exosomes and ectosomes are not rigid and thus further characterization techniques are needed to improve the description of vesicular bodies.

Table 1.2: **Summary of recent studies in EVs in ALS.** Abbreviations: ALS amyotrophic lateral sclerosis, SALS sporadic ALS, MND motor neuron disease, NTA nanoparticle tracking analysis, TEM transmission electron microscopy, EVs extracellular vesicles, ELISA enzyme-linked immunosorbent assay, WB western blot, ab antibody, EXOs exosomes, MVs microvesicles, CSF cerebrospinal fluid, ADEs astrocyte-derived exosomes.

Author	Year	Sample	Patients	Methods	EVs Isolation/enrichment	EVs type	EVs concentration	Molecule/s of interest	Conclusion
Banack et al. [44]	2020	Peripheral blood	Probable or definite ALS/MND	ExoQuick, NTA	L1CAM ab (mouse anti-human CD171) biotinylated, CD81 ELISA	Neural-enriched fraction of EVs with characteristics consistent with exosomes	CD81: 5.2-8.7x10^{12} particles/mL; CD63: 7.4-13.7x10^{12} particles/mL	miRNAs	8 miRNA sequences differentially expressed in ALS/MND and controls.
Chen et al. [45]	2019	Peripheral blood	SALS	ExoQuick, TEM	ACSA-1 ab biotinylated	Enriched Astrocyte-derived exosomes	NA	IL-6	IL-6 in ADEs of ALS patients increased and positively associated with the rate of disease progression.
Pregnolato et al. [46]	2021	Peripheral blood	SALS and ALS (TDP-43)	miRCURY Exosome Isolation Kit, TEM	miRCURY Exosome Kit	Enriched EXOs, verified by TEM and WB	NA	miRNAs	No significant differences between ALS and controls were revealed. It was a pilot study.
Sproviero et al. [32]	2018	Peripheral blood	SALS	Ultracentrifugation (differential centrifugation and filtration), NTA, TEM	Ultracentrifugation, WB analysis	MVs and EXOs confirmed through WB (Annexin V, Integrin $\alpha 2\beta$, Alix, Flotillin)	10^7-10^9 particles/mL	Proteins (SOD-1, TDP-43, FUS)	MVs and EXOs from ALS patients were significantly bigger than controls; significant enrichment of SOD1, TDP-43, p-TDP-43 and FUS in MVs of ALS compared to control; EXOs cargo similar in ALS and control. SOD1 enriched in EXOs compared to MVs, p-TDP-43 and FUS slightly more concentrated in MVs than EXOs.
Thompson et al. [47]	2020	Cerebrospinal fluid	ALS	Ultrafiltration liquid chromatography, NTA, TEM	Ultrafiltration liquid chromatography	Mixed population of EVs	2x10^8-2x10^9 particles/mL	Proteins (1020 identified and quantified)	CSF EVs size distribution and number are similar in ALS and healthy controls and in ALS patients with and without a *C9orf72* hexanucleotide repeat expansion
Vassileff et al. [48]	2020	Post-mortem tissues	ALS	Ultracentrifugation (differential and gradient centrifugation), NTA, TEM	Ultracentrifugation, markers analysis (flotillin-1, Tsg191 and syntenin)	Motor cortex extracellular vesicles (small EVs)	NA	Proteins (TDP-43)	12 unique proteins found in ALS EVs compared to controls (CD177, CHMP4B, CSPG5, DYNC1I2, IGHV3-43, LBP, RPS29, S100A9, SAA1, SCAMP4, SCN2B and SLC16A1)
Yelick et al. [49]	2020	Cerebrospinal fluid	ALS (different progression)	Total Exosome Isolation Reagent (previous filtration and centrifugation)	Total Exosome Isolation Reagent	Enriched EXOs	ALS: 8.8x10^8 particles/mL; Control: 11x10^8 particles/mL	miR-124-3p	Possible potential of CSF exosomal miR-124-3p in the indication of disease progression of ALS.
		Lumbar cord tissue (mice)	SOD1G93A mice	CD63-GFPf/f, confocal microscopy	No isolation, only detection				

Most of the studies mentioned in Table 1.2 focus on studying the presence of ALS related miRNAs or proteins and aim to find a useful biomarker for ALS/MND. Additionally, pathological proteins, such as SOD-1, TDP-43 and FUS were found in both, ectosomes and exosomes [32] supporting the hypothesis of cell-to-cell propagation via EVs.

There were also some proteins that were exclusively present in ALS motor cortex EVs and not in the corresponding neurological controls; some other proteins were also identified to be statistically significant differentially expressed between ALS motor cortex EVs and controls, but it was not the case for total brain sample [48].

In these studies, the presence of EVs was confirmed via TEM [32, 45–48], studying the morphology and size of EVs.

The group led by Dr. Brites has focused on studying miRNAs related to ALS and AD. On their research, they have found out that the overexpression of miR-124 plays a key role in pathological processes related to ALS [50]. They have also identified miR-155 as a promising marker to track ALS [51] and are testing the modulation of these miRNAs as an approach to treat ALS [52]. Interestingly, Yelick et al. [49] also pointed exosomal miR-124-3p as a potential indicator of ALS progression.

1.1.7 Alternative models in the study of ALS

One of the greatest problems that the study of ALS faces is that the main source of pathological information from patients comes from neural tissue obtained post-mortem. This tissue, normally represents the advanced stages of the disease, making it difficult to decipher the mechanisms that lie underneath the pathologies of the disease. In conclusion, different models are needed for the study of ALS.

Rodent models are the most widely used ALS models to study the disease mechanism and to test potential treatments [53]. However, most of these models fail to emulate the human disease. The most common model used in ALS study is the $SOD1^{G93A}$ mouse [54]. The problem of using this model is that the majority of patients are diagnosed with SALS, which may or may not develop abnormal SOD1 protein, resulting in no correlation between the models and the patients. Recently, some TDP-43 expression models have also been developed [23], however, they have presented some difficulties in recapitulating the disease and are still not widely used as ALS models.

There are different model systems for different genetic subtypes of ALS apart from rodent models, including yeasts, zebra fish, *Caenorhabditis elegans* and *Drosophila*. However, these models are unable to mimic the whole characteristics of the human disease.

Recent studies are using peripheral tissues in the study of ALS and have proven their utility, being able to reproduce some pathological features of the disease, such as the abnormal phosphorylation of TDP-43 in immortalized lymphocytes obtained from patient

cells [55]. Induced pluripotent stem cells (iPSC)-derived neurons are arising as a novel technology to study neurons from patients [56]. However, most of the current studies utilize cells obtained from FALS patients, which represent just a 10% of the ALS cases.

2 Project Background

The group led by Dr. Martín Requero has studied and stablished a lymphoblastic model derived from ALS patients. These cells can be obtained from a sample of blood, which contains peripheral blood mononuclear cells (PBMCs), that include B lymphocytes. To obtain the immortalized lymphoblasts, PBMCs were isolated and incubated with the Epstein-Barr virus which interacts with the CD21 receptor of B lymphocytes, infecting these cells.

In their studies, they show that immortalized lymphocytes from SALS patients recapitulate the TDP-43 abnormalities observed in neuronal cells of ALS cases, including translocation from nucleus to cytoplasm, truncation, and hyperphosphorylation [55].

The phosphorylation of S409/410 of TDP-43 is a highly consistent feature in pathologic inclusions in the spectrum of TDP-43 proteinopathies [57]. Protein CK-1δ is considered the main kinase involved in TDP-43 phosphorylation [58]. Consequently, the group led by Professor Martínez has developed a number of CK-1δ inhibitors (e.g. IGS-2.7), able to prevent TDP-43 phosphorylation in vitro and neurotoxicity in vivo [59, 60].

In addition, the results from Posa et al. [55] indicate that the inhibition of CK-1δ prevents the cytosolic accumulation of TDP-43, as well as reducing the concentration of phosphorylated TDP-43, recovering its usual proteostasis.

In conclusion, these lymphoblastic lines are a validated ALS disease model obtained directly from patients.

3 Hypothesis and objectives

3.1 Hypothesis

The hypothesis of this project is based on the assumption that EVs can inform on the pathological status of ALS patients and also in the efficiency of drugs.

3.2 Objectives

Considering the hypothesis, the objectives planned for this project are:

- To characterize EVs from ALS patients' models and healthy controls regarding:
  - size
  - concentration
  - membrane markers
  - biomolecule load
- To determine whether ALS related drugs modulate EVs population, reflecting changes in these parameters.

4 Materials and Methods

4.1 Cell lines

Lymphoblastic cell lines were donated by Dr. Martín Requero. To obtain the lymphoblastic lines, B lymphocytes were isolated utilizing Lymphoprep™ density gradient medium. The resulting cells were incubated with Epstein-Barr Virus donated by Longina Akhatat (National Institute of Alcohol and Abuse Disorders, NIH, Bethesda, USA). Control cells were obtained from healthy donors and have been named C105, C106, C110, C126. Patient cells were obtained from SALS patients and have been named E2, E4, E6, E8 and E10.

4.2 Cell lines maintenance

Lymphoblastic cell lines were incubated in gibco RPMI-1640 media with L-glutamine (2 mM) supplemented with gibco 10% exosome depleted FBS and gibco penicillin-streptomycin (100 µg/mL) in a wet incubator with 5% CO_2 at 37 ºC.

4.3 Treatments

The treatment consists of 5 µM of a CK-1δ inhibitor, IGS-2.7, a compound derived from N-Benzothiazolyl-2-phenyl-acetamide, for 48 h. This compound was synthesized by the laboratory of Professor Martínez [59]. In the case of controls, the vehicle, dimethyl sulfoxide (DMSO) was added instead.

4.4 Extracellular vesicles isolation

The EVs produced by the lymphoblasts were isolated utilizing the Thermofisher Total Exosome Isolation Reagent. The samples were resuspended in 50 µL of PBS with EDTA (5 mM) and further diluted (2:900 in PBS with EDTA) for the NTA. PBS 10X was obtained

from Fisher Bioreagents (#BP665-1), Ethylenediaminetetraacetic acid (EDTA) disodium salt, dihydrate, for molecular biology from Scharlau (#AC09610250).

4.5 Nanoparticle Tracking Analysis

For each sample, 4 videos of 60 seconds were recorded and analyzed on the NanoSight NTA software, which calculated the concentration and size of the particles. The instruments used were The Malvern Panalytical NanoSight LM10 and NS300. In fluorescence mode, the settings were adjusted to have a cutoff of 50 and 70 nm, so that single QD would not be counted in the analysis.

4.6 Transmission Electron Microscopy

A control and a patient sample were visualized using TEM. In order to prepare the grids for the measurements, they were glow discharged in a Quorum GloQube® equipment for 10 seconds at 20 mA. After preparing the grids, a drop of sample was added (about 6 µL) and left to dry for 20 minutes. Then, the grids were washed three times in PBS buffer and fixated with 1% glutaraldehyde. Finally, the samples were washed with water and stained with uranyl acetate.

The measurements were carried out in a JEOL JEM-1230 microscope by the Electron Microscopy Facility at the Biological Research Center Margarita Salas (Spanish National Research Council).

4.7 Atomic Force Microscopy

With the purpose of finding the most optimal conditions for the assay, two different immobilization methodologies found in the bibliography [61, 62] were tested. On the first one, the sample was immobilized on a mica surface. In order to do so, the mica was cleaved and treated with 10 mM $NiCl_2$ for 10 seconds. After rinsing the surface with miliQ water and drying it with N_2, a drop of the EVs sample (20 µL) was placed on the mica. The lid was sealed inside a petri dish and left at 4 ºC overnight. The following day, the surface was rinsed with PBS three times before adding 80 µL of fresh PBS to cover the sample. For the second methodology, a glass cover was cleaned and treated with 1% (w/v) poly-L-lysine for 1 hour. The glass cover was rinsed with miliQ water and dried overnight at 37 ºC. Lastly, 320 µL of sample were added on top of the poly-L-lysine for the measurements.

The measurements were carried out in a commercial atomic force microscopy (AFM) system (JPK Nanowizard 2, Bruker) by Dr. Pedraz in intermittent contact (dynamic) mode using scanning by probe configuration in liquid. Triangular silicon cantilevers

MSNL-10-A (Bruker) were used with a tip radius of 2 nm, nominal spring constant of 0.07 N/m and a resonance frequency in air of around 22 kHz.

4.8 Western blot

Laemmli buffer was added to the samples and after heating them for 5 min at 95 ºC, they were run in a 4-20% Mini-PROTEAN TGX Precast Protein Gel via electrophoresis. The proteins were transferred from the gel to a PVDF membrane utilizing the Trans-Blot Turbo Transfer System (Bio-Rad), and the Trans-Blot Turbo Mini 0.2 µm Nitrocellulose Transfer Pack. The membrane was then incubated with the primary antibody (ProteinTech rabbit anti-TDP-43 #10782-2AP) in a 1:1000 milk dilution overnight. Next, the membrane was washed 3 times with 5% milk for a total of 30 min. Then, the incubation with the secondary antibody (Bio-Rad HRP-conjugated anti-rabbit IgG #1706515) was carried out in a 1:5000 TBST dilution for 1 h and the membrane was washed 3 times with TBST for a total of 30 min. Pierce ECL Western Blotting Substrate was used to detect HRP activity in the ChemiDoc Imaging System. Quantification was performed using ImageJ software. Running Buffer consisted of Tris Glycine (10 mM Tris and 100 mM Glycine), 0.1% SDS and distilled water. TBST consisted of 20 mM Tris, 150 mM NaCl, 0.02% Tween and distilled water. Tris was obtained from Thermo Scientific (#17926); Glycine, 99% from Thermo Scientific (#A13816); SDS from Bio-Rad (#1610301). CD63 polyclonal antibody was obtained from ProteinTech (#25682-1-AP) and used in a 1:1000 dilution.

4.9 Fluorescent labelling

Streptavidin-conjugated QD (Invitrogen™) were incubated with 2 µL of biotinylated antibody (BioLegend Biotin anti-human CD63 Antibody #353017, or Invitrogen™ anti-mouse IgG #31903 for controls) and 46 µL of PBS (1% goat serum) for 2 h in a rotating mixer. Then, they were added to 2 µL of sample, and they were incubated overnight in a rotating mixer. The following day, the sample was further diluted with 850 µL of PBS. The final concentration of QD was 9 nM.

4.10 miRNA detection via Cas13 in vitro activity

In order to form the ribonucleoprotein (RNP), Cas13a (E124) was incubated at 37 ºC for 30 min with the crispr ribonucleic acid (crRNA) oligonucleotides which were designed to hybridize with the target miRNAs hsa-miR-124-3p and hsa-miR-155-5p. The final concentration of RNP was 50 nM (in a 1:1 molar ratio Cas13:crRNA). After the incubation, RNAse Alert was added to each well, as well as the desired volume of RNP. Finally, synthetic miRNA was added at different concentrations (25 nM, 30 nM, 40 nM,

50 nM and 100 nM) before reading the plate in a Synergy H4 Hibrid Reader exciting the samples at 490 nm and measuring emission at 530 nm. The positive control is a region of the R gene of SARS-CoV-2. The crRNAs and synthetic miRNAs were obtained from IDT and their sequences can be found in Table 4.1.

Table 4.1: **RNA sequences obtained from IDT.** Abbreviations: crRNA crispr ribonucleic acid.

RNA	Sequence
hsa-miR-124-3p	UAAGGCACGCGGUGAAUGCC
crRNA 124-3p	GATTTAGACTACCCCAAAAACGAAGGGGACTAAAAC GGCAUUCACCGCGUGCCUUA
hsa-miR-155-5p	UUAAUGCUAAUCGUGAUAGGGGU
crRNA 155-5p	GATTTAGACTACCCCAAAAACGAAGGGGACTAAAAC ACCCCUAUCACGAUUAGCAUUAA
Orf12b SARS-CoV-2 (Control R)	GGCGAAGUUGUAGGAGACAUUAUACUUAAACCAGCAAAU AAUAGUUUAAAAAUUACAGAAGAGGUUGGCCACACAGAU CUAAUGGCUGCUUAUGUAGACAAUUCUAGUCUUACUA
crRNA Control R	GAUUUAGACUACCCCAAAAACGAAGGGGACUAAAAC CCAACCUCUUCUGUAAUUUUUAAACUAU

4.11 miRNA agarose gel electrophoresis

The synthetic miRNAs and the crRNAs were run on a 12% polyacrylamide gel-8 M urea for 1 hour at 120 V. The gel was done by mixing 4.8 g of urea, 1 mL of TBE 10X, 3 mL acrylamide 40%, and H_2O DEPC up to 10 mL. Finally 50 µL APS 10% and 6 µL TEMED are added. The samples were dyed with SYBR Gold and loaded with formamide. Bis-Acrylamide 19:1 40% was obtained from Fisher Bioreagents (#BP1406-1), Urea GR for analysis (ACS, Reag. Ph Eur) from Merck (#1084871000), Boric acid for analysis, (ExpertQ®, ACS, ISO, Reag. Ph Eur) from Scharlab (#AC05780500), Tris base from Fisher Bioreagents (#BP152-500), the formamide was taken from the MEGAscript™ T7 transcription kit from Invitrogen™ (#AM1334).

4.12 miRNA detection using Quantum Dot-Based Förster Resonance Energy Transfer

The detection method is based on a methodology found in the bibliography [63]. The methodology is based on ribonucleic acid (RNA) and deoxyribonucleic acid (DNA) base

pairing and stacking. The capture sequence binds to QD via streptavidin-biotin binding and is complementary to a part of the reporter DNA. The reporter sequence is composed of two parts, one is complementary to the capture sequence and the other one is complementary to the miRNA sequence. The reporter sequence binds to terbium (Tb) via streptavidin-biotin binding. The capture sequence was designed to have a low melting temperature (16.5 ºC) so that it does not form stable double-strands by pairing with the reporter sequence unless the miRNA is present (due to nick stacking). For the measurements, the Tb is excited and due to its proximity to the QD in the double-stranded complex, the Förster or fluorescence resonance energy transfer (FRET) process occurs. The Tb-DNA and QD-DNA conjugates were obtained by mixing Tb-streptavidin or QD525-streptavidin with biotin labelled oligonucleotides in Tris-Cl buffer. The mixtures were incubated overnight while rotating. The Tb-DNA were purified three times by Zeba™ Spin Desalting Columns, 7K MWCO. Synthetic miRNA was added in increasing concentrations (0, 5 and 10 nM). The measurements were taken in a Synergy H4 plate reader. The excitation was performed at 337 nm and the emission at 494 nm and 525 nm with a delay of 500-900 µs. The FRET ratio has been calculated as the measurement at 494 nm (Tb emission) divided by the measurement at 525 (QD525 emission) and the data has been normalized to be between 0 and 100. Tris-Cl buffer consisted of 20 mM Tris and 500 mM NaCl (pH 8.0). QD-streptavidin was obtained from Invitrogen™. Streptavidin-Tb cryptate was obtained from cisbio (Ref 610SATLF). Zeba™ Spin Desalting Columns, 7K MWCO were obtained from Thermo Scientific. The synthetic DNA was obtained from IDT and the sequences can be found in Table 4.2.

Table 4.2: **RNA sequences obtained from IDT.** Abbreviations: DNA deoxyribonucleic acid.

DNA	Sequence
reporter 155-5p	ACCCCTATCACGATTAGCATTAA-CTATGACAG-biotin
capture 155-5p	biotin-CTGTCATAG

4.13 Statistical Analysis

The NTA experiments were repeated three times for each patient sample (except for E8). Statistical significance was calculated utilizing the ordinary one-way ANOVA for multiple comparisons in GraphPad Prism 9.3.1. The comparison has been made between the mean of each group. Significative differences have been marked with * for $p < 0.05$ and # for $p < 0.1$. The graphical representations include the standard error of the mean (SEM).

5 Results and discussion

In order to characterize EVs from the lymphoblastic models, lymphoblasts derived from SALS patients and healthy controls were incubated in RPMI media. Upon reaching a concentration of 2 million cells, the cells were treated as specified in section 4.3.

Firstly, the EVs produced by the lymphoblasts were isolated utilizing a vesicle precipitating kit. The samples were resuspended in PBS for the NTA measurements. For each sample, 4 videos were recorded and analyzed, calculating the concentration and size of the particles. The results of the NTA are shown in the section 5.1. The presence of EVs was confirmed through microscopy techniques (section 5.2).

Secondly, a preliminary study of the contents of TDP-43 in EVs from lymphoblastic models was carried out via western blot. The resulting image and analysis can be seen in section 5.3.

An early approach to fluorescently label EVs with QD was performed. The tetraspanin CD63 was selected. The labelled EVs were analyzed using the fluorescence mode in the NanoSight to perform a NTA. The results are shown in Figure 5.7B.

Finally, alternative methods have been tested to detect synthetic miRNA and are discussed in section 5.5, since specific miRNAs have been found to be related to neurodegenerative diseases. The detection of these small molecules is not always easy and normally involves the use of specific adapters in quantitative polymerase chain reaction (qPCR). In this section, two different methodologies have been attempted to quantify miRNA in EVs without polymerase chain reaction (PCR).

5.1 Effects of IGS-2.7 on extracellular vesicles production and size

The concentration and the size of the EVs produced by control and SALS-patient derived lymphoblasts were studied via NTA. The Figure 5.1B shows the effects of IGS-2.7 on EVs production and size.

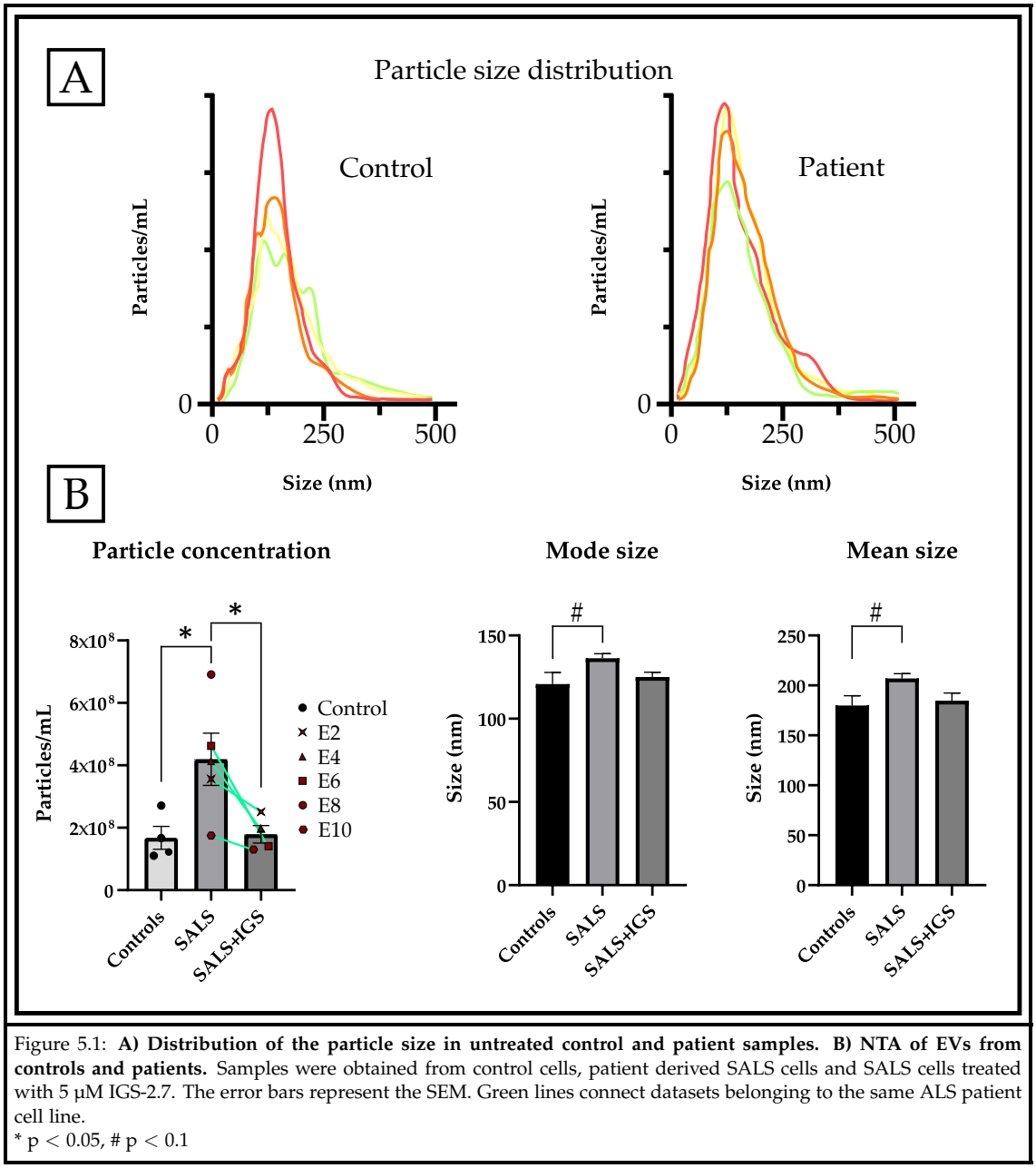

Figure 5.1: **A) Distribution of the particle size in untreated control and patient samples. B) NTA of EVs from controls and patients.** Samples were obtained from control cells, patient derived SALS cells and SALS cells treated with 5 µM IGS-2.7. The error bars represent the SEM. Green lines connect datasets belonging to the same ALS patient cell line.
* $p < 0.05$, # $p < 0.1$

As seen in Figure 5.1B, the concentration of EVs is significantly higher on the EVs produced by SALS lymphoblast than on the EVs produced by control lymphoblasts, and it is significantly reduced upon treatment with IGS-2.7. The same applies to the mean and mode size of the EVs, which are higher on EVs produced by SALS lymphoblast, and are reduced when treated with IGS-2.7.

5.2 EVs evaluation via microscopy

In order to confirm the presence of EVs in the samples, a control (C110) and a patient sample (E2) were evaluated by TEM and AFM.

5.2.1 EV samples visualization on TEM

The samples were observed via TEM with a 60000X magnification. The resulting micrographs can be seen in Figure 5.2.

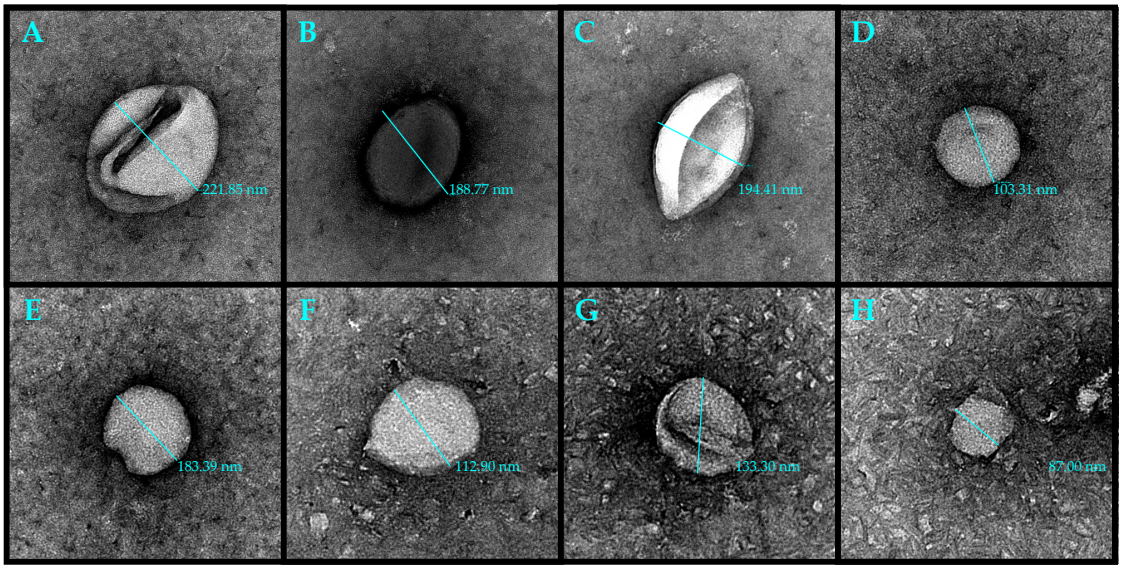

Figure 5.2: **A-D EVs from control sample. E-H EVs from SALS sample.** The EVs in the images have been measured and are in the size range of exosomes and ectosomes (measured diameters are between 80 and 230 nm).

The images show some rounded membrane-like structures with a diameter that corresponds to the size range of EVs. These results demonstrate the presence of particles with morphology and size consistent with EVs in the visualized samples.

5.2.2 EV samples visualized on AFM

Atomic force microscopy was used in order to study the topography of the EVs inside the used medium. Two different techniques were used when immobilizing the EVs for their visualization in the AFM with the purpose of finding the most optimal conditions for the assay. One implied the use of poly-L-lysine to immobilize the sample in glass [62], while the other one used $NiCl_2$ on a mica surface [61]. A comparison between these methodologies using the same EVs control sample can be seen in Figure 5.3.

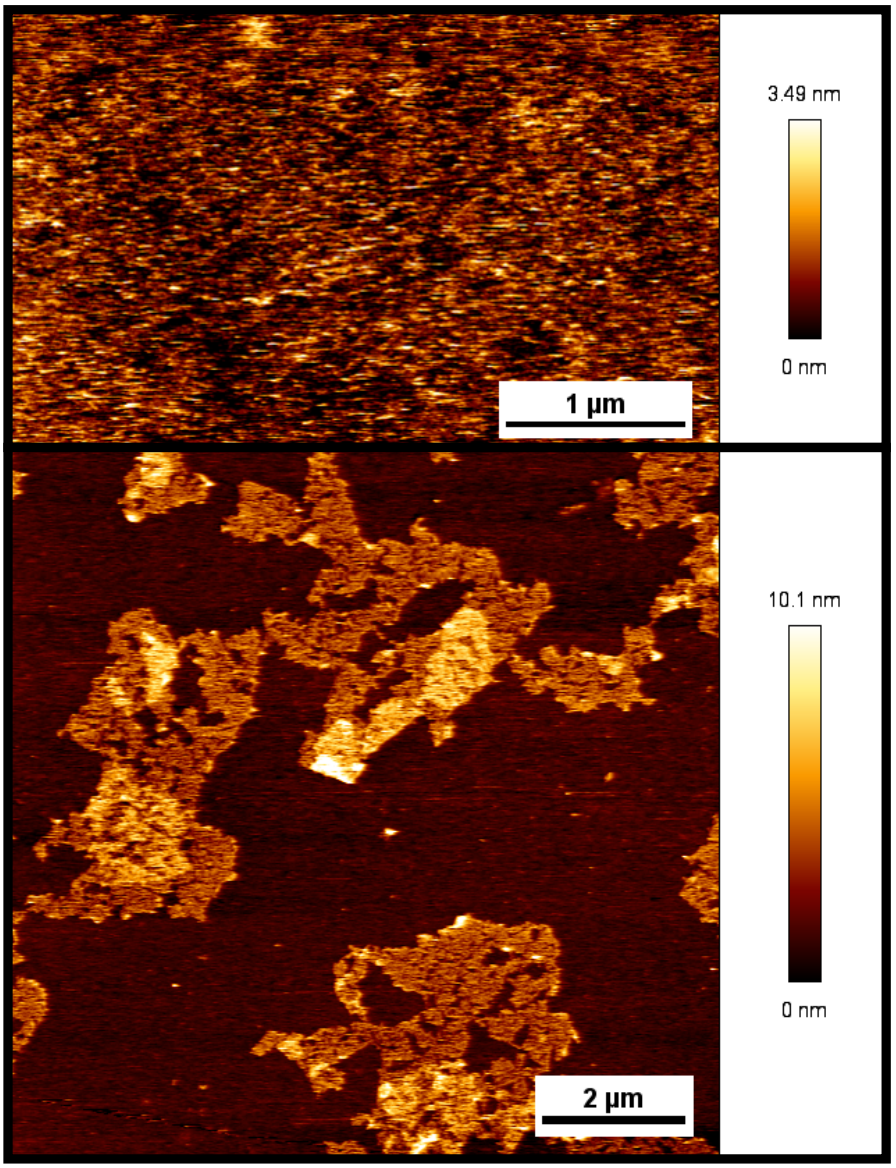

Figure 5.3: **EVs from control sample immobilized on glass (upper image) and on mica (lower image).** The images cover 4x4 µm^2 of surface (upper image) and 10x10 µm^2 (lower image).

The image obtained from the sample immobilization on glass does not show any visible structures attributable to extracellular vesicles. This may indicate that this methodology is not efficient enough for a dynamic mode measurement of EVs (upper image of Figure 5.3). On contrast, the sample immobilized on mica seems to have some kind of cellular debris which can be observed in the larger scan (lower image of Figure 5.3).

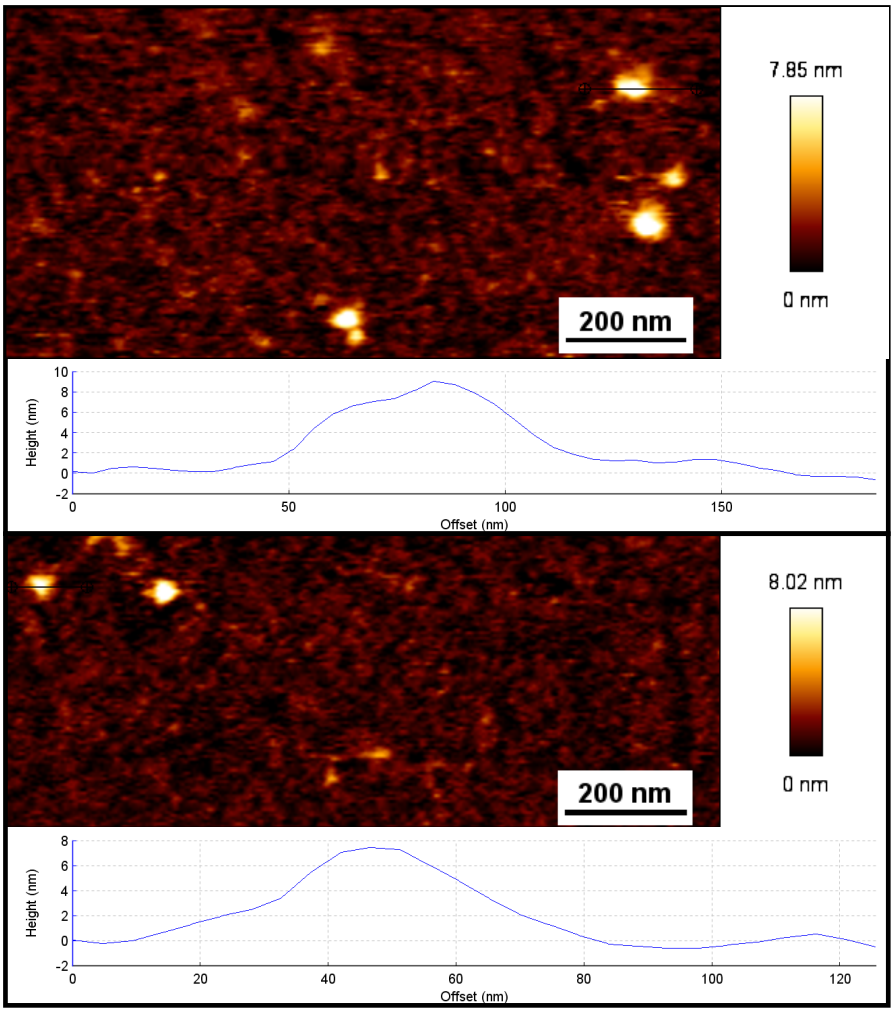

Figure 5.4: **Closer view of the control sample immobilized on mica and height profiles.** The feature height is around 6-8 nm and the diameter around 60 nm.

When taking a closer look into this sample, as shown in Figure 5.4, some small features appear (around 6-8 nm in height) with a diameter comparable to an exovesicle size (around 60 nm). Even though the results are similar to those obtained in other studies [61], the technique does not allow to confirm whether these would be EVs.

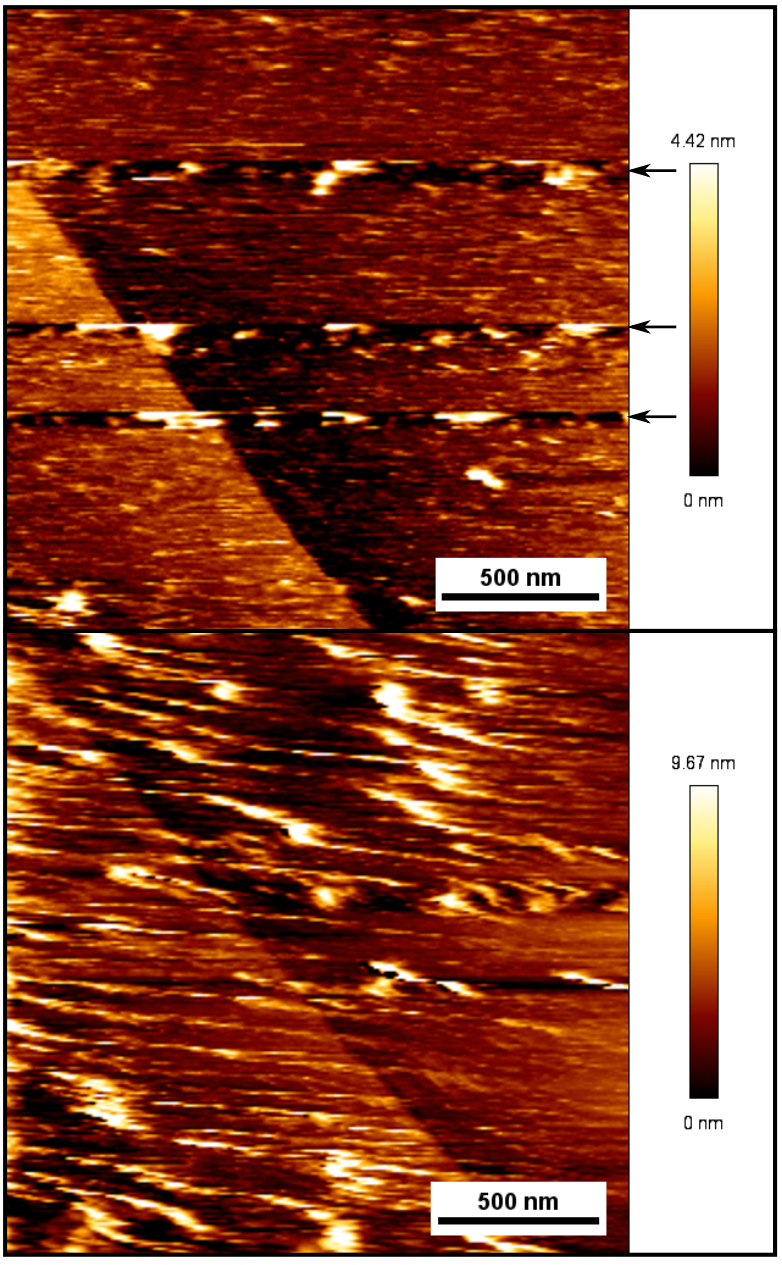

Figure 5.5: **EVs from SALS sample immobilized on mica.** The arrows are marking the regions in which the tip lost contact with the surface. The images were taken with different forces, using a lower force in the lower image.

The image obtained from the immobilized patient sample on mica has been marked with three arrows (upper image of Figure 5.5) on specific regions where the tip started to loose contact with the surface. In these regions higher features are appreciated but not properly defined. These might probably be part of EVs being displaced by the tip

in the dynamic mode (i.e. tapping), and become more evident when reducing the force applied to the surface (lower image of Figure 5.5).

The AFM images may be showing EVs that successfully got immobilized and shrank through the process resulting in a low height (6 to 8 nm). However, it could also be that the EVs are being displaced by the tip due to the tapping mode, as pointed by Figure 5.5, where the minimum required force to maintain the contact for measurements is large enough to move some features. In order to confirm if these features which seem to be loosely attached to the surface are actually EVs, the samples should be measured in a spectroscopy based mode (ie. PeakForce Tapping®, QI®, Jumping mode®), which allows a very accurate control on the applied force and avoids the presence of lateral dragging forces. However, this mode is unavailable in the equipment used for this project.

5.3 Effects of IGS-2.7 on TDP-43 carried in extracellular vesicles

An initial study of TDP-43 concentration in EVs has been done by western blot analysis. The results are shown in Figure 5.6.

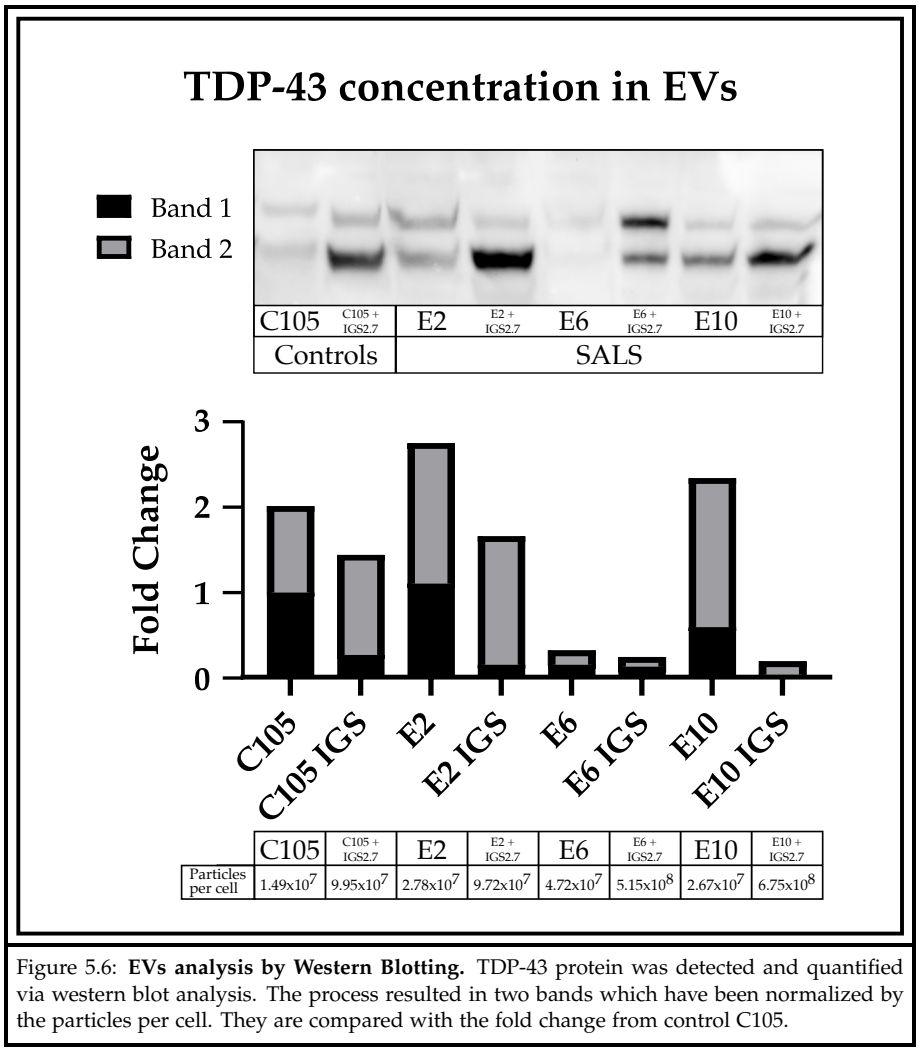

Figure 5.6: **EVs analysis by Western Blotting.** TDP-43 protein was detected and quantified via western blot analysis. The process resulted in two bands which have been normalized by the particles per cell. They are compared with the fold change from control C105.

From these results, it is clear that, upon treatment with IGS-2.7, the concentration of TDP-43 is decreased in the EVs. This is in concordance with the behavior that occurs in cells. The results from Martínez-González et al. [64] show that IGS-2.7 recovers TDP-43 homeostasis by decreasing its phosphorylation and enhancing the nuclear localization in ALS derived lymphoblasts.

The membranes were incubated with anti-CD63 antibody. However, no signal was detected when using this antibody. This could be due to the low concentration of this protein in the EVs membranes, since the isolation reagent used does not exclusively

isolate vesicles containing CD63.

5.4 Fluorescent labelling of CD63

As a first approach to fluorescently label membrane proteins from EVs, CD63 was marked with a biotinylated antibody which interacts with streptavidin-QD. The labelling process is schematically represented in Figure 5.7A. The resulting samples were measured in the NanoSight and the concentration of labelled EVs is represented in Figure 5.7B.

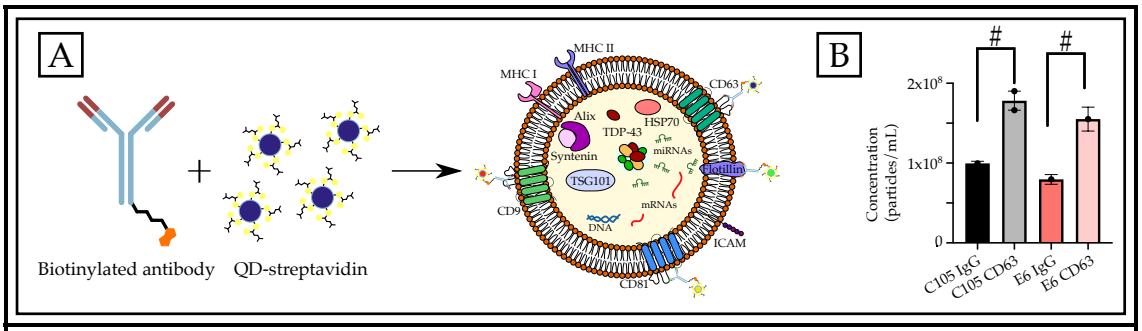

Figure 5.7: **A) Schematic representation of EVs labelling using QD.** Biotinylated antibody interacts with membrane proteins, such as tetraspanins and with the Quantum Dot nanoparticles via biotin-streptavidin binding. **B) Concentration of fluorescent particles in control samples.** The samples incubated with IgG represent the negative control. # $p < 0.3$

The Figure 5.7B shows that the QD have successfully marked the targeted membrane marker. However, it seems that the concentration of CD63 in EVs is very low (it was undetected in the western blot) resulting in a very low percentage of EVs being labelled. A different membrane protein should be selected to acquire a higher percentage of labelling.

5.5 miRNA detection

Regarding the detection of miRNA in samples, different approaches were tested. First, a Cas13 in vitro activity detection assay utilizing synthetic miRNA was carried out. The result is shown in Figure 5.8

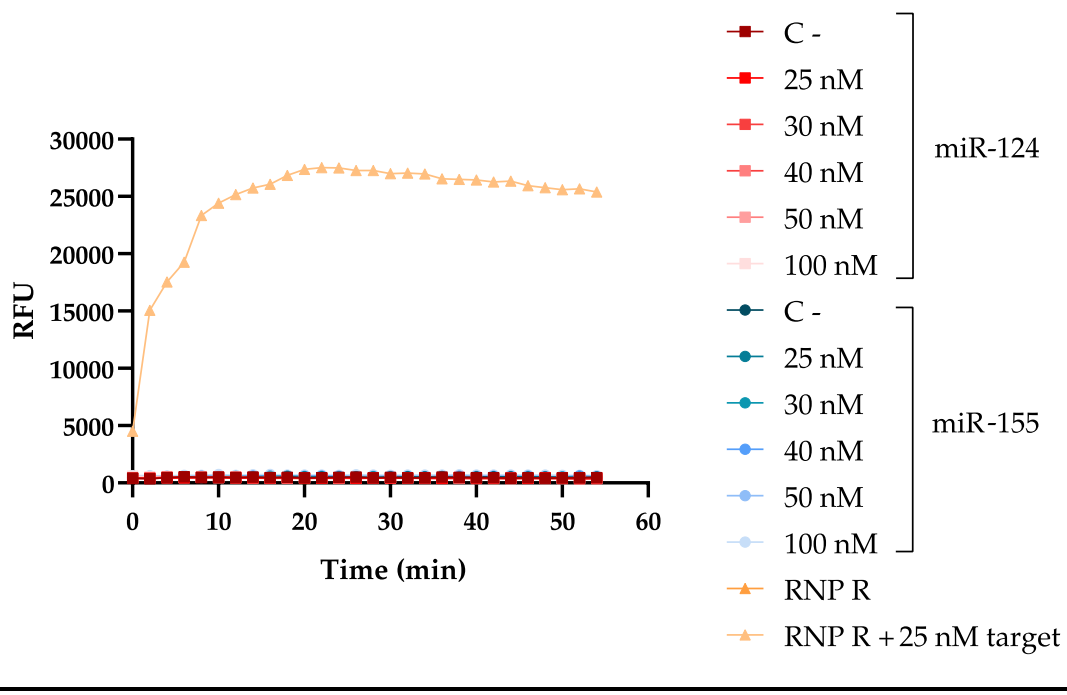

Figure 5.8: **Cas13 in vitro activity detection assay.** Different concentrations of synthetic miRNA (both 155 and 124) were tested. R with 25 nM target is a positive control. Abbreviations: RFU relative fluorescence units, miRNA micro ribonucleic acid.

Since no miRNA was detected utilizing this method (apart from the positive control), an agarose gel electrophoresis was performed to confirm the presence of miRNA in the obtained synthetic samples. The electrophoresis can be seen in Figure 5.9

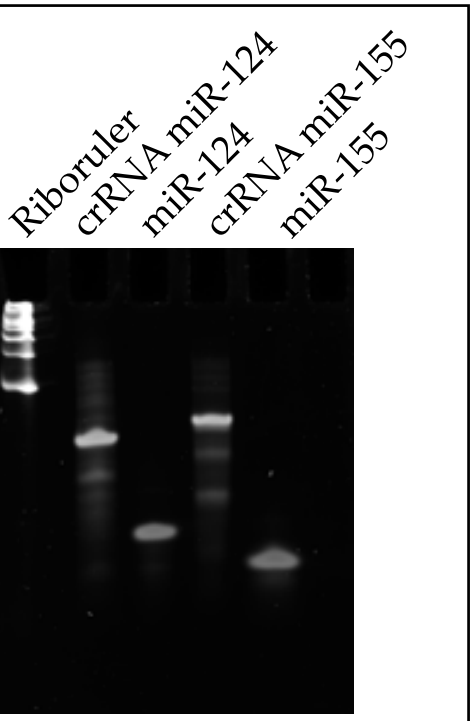

Figure 5.9: **RNA agarose gel electrophoresis** The synthetic miRNAs and crRNAs were run in a 12% polyacrylamide gel-8 M urea.

The gel shows that there is miRNA in the samples, so the problem is probably due to the small size of the miRNA and the crRNA leading to problems in the sequence recognition during the RNP formation.

Finally, another miRNA detection method using QD was tested. This method is based on the hybridization of miRNA to its complementary DNA sequence which is bound to Terbium (reporter) and the hybridization of a sequence complementary to the reporter, which is bound to a QD. A schematic representation can be found in Figure 5.10A. The result is represented in Figure 5.10B.

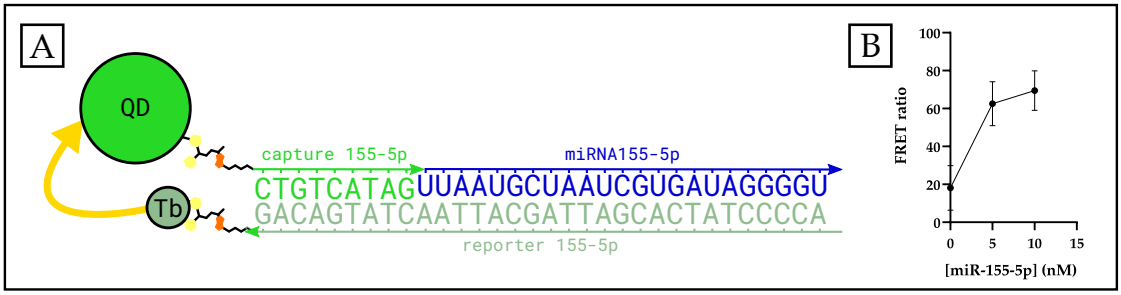

Figure 5.10: **A) Schematic representation of miRNA detection utilizing QD-based FRET.** When the hybridization occurs, the Tb and the QD are in proximity, enabling the FRET process. **B) miRNA concentration detection by QD/Tb FRET ratio.** Increasing concentration of synthetic miR-155-5p leads to an increased signal of the QD/Tb FRET ratio. The error bars represent the SEM.

The preliminary result shown in Figure 5.10B shows that the miR-155-5p could be detected using this methodology. However, it would require more tests with a wider range of miRNA concentration and more repetitions, since it currently has a considerable error.

6 Conclusion

The aim of this project was to characterize EVs produced by ALS patients' models and healthy controls, and their modulation upon pharmacological treatment. The characteristics studied have been their size, concentration, membrane markers, and biomolecule load.

The NTA has determined that the concentration of EVs produced by SALS lymphoblasts is significantly higher than the concentration of EVs produced by healthy controls. Upon treatment with the CK-1δ inhibitor IGS-2.7, the concentration of EVs is significantly reduced. According to the results, there is a tendency for the SALS lymphoblasts to produce bigger EVs that appears to be modulated by pharmacological treatment.

Additionally, microscopy techniques have been used to confirm the presence of EVs in the samples and measure their diameter.

The protein selected to fluorescently label EVs was CD63. This protein was labelled with QD, and the labelling was analyzed with NTA. However, this protein could not be detected via western blot in the samples, probably because its concentration in these membranes is very low, resulting in a low percentage of EVs being marked.

Finally, the presence of ALS related biomolecules was studied by western blot, to detect TDP-43, and through different miRNA detection assays. Regarding the TDP-43 concentration, it is clear that it is reduced upon treatment with IGS-2.7. The concentration of synthetic miRNA was preliminarily detected by a time-gated FRET assay.

Bibliography

[1] Orla Hardiman et al. "Amyotrophic lateral sclerosis". In: *Nature Reviews Disease Primers* 3.1 (Oct. 2017). DOI: 10.1038/nrdp.2017.71. URL: https://doi.org/10.1038/nrdp.2017.71.

[2] Pilar Rojas et al. "Amyotrophic Lateral Sclerosis: A Neurodegenerative Motor Neuron Disease With Ocular Involvement". In: *Frontiers in Neuroscience* 14 (Sept. 2020). DOI: 10.3389/fnins.2020.566858. URL: https://doi.org/10.3389/fnins.2020.566858.

[3] Sara Zarei et al. "A comprehensive review of amyotrophic lateral sclerosis". In: *Surgical Neurology International* 6.1 (2015), p. 171. DOI: 10.4103/2152-7806.169561. URL: https://doi.org/10.4103/2152-7806.169561.

[4] Sarah Martin, Ahmad Al Khleifat, and Ammar Al-Chalabi. "What causes amyotrophic lateral sclerosis?" In: *F1000Research* 6 (Mar. 2017), p. 371. DOI: 10.12688/f1000research.10476.1. URL: https://doi.org/10.12688/f1000research.10476.1.

[5] Elisa Longinetti and Fang Fang. "Epidemiology of amyotrophic lateral sclerosis: an update of recent literature". In: *Current Opinion in Neurology* 32.5 (Oct. 2019), pp. 771–776. DOI: 10.1097/wco.0000000000000730. URL: https://doi.org/10.1097/wco.0000000000000730.

[6] Jack J. Chen et al. "Overview of current and emerging therapies for amytrophic lateral sclerosis". In: *The American Journal of Managed Care* 26.Suppl 9 (Aug. 2020), S191–S197. DOI: 10.37765/ajmc.2020.88483. URL: https://doi.org/10.37765/ajmc.2020.88483.

[7] Thomas M. Jenkins, Hannah Hollinger, and Christopher J. McDermott. "The evidence for symptomatic treatments in amyotrophic lateral sclerosis". In: *Current Opinion in Neurology* 27.5 (Oct. 2014), pp. 524–531. DOI: 10.1097/wco.0000000000000135. URL: https://doi.org/10.1097/wco.0000000000000135.

[8] Nicholas T. Bott et al. "Frontotemporal dementia: diagnosis, deficits and management". In: *Neurogenerative Disease Management* 4.6 (Dec. 2014), pp. 439–454. DOI: 10.2217/nmt.14.34. URL: https://doi.org/10.2217/nmt.14.34.

[9] Gabriele Cipriani et al. "Is that schizophrenia or frontotemporal dementia? Supporting clinicians in making the right diagnosis". In: *Acta Neurologica Belgica* 120.4 (Apr. 2020), pp. 799–804. DOI: 10.1007/s13760-020-01352-z. URL: https://doi.org/10.1007/s13760-020-01352-z.

[10] Laura de Godoy Rousseff Prado et al. "C9ORF72 and the FTD-ALS spectrum: a systematic review of neuroimaging studies". In: *Dementia & Neuropsychologia* 9.4 (Dec. 2015), pp. 413–421. DOI: 10.1590/1980-57642015dn94000413. URL: https://doi.org/10.1590/1980-57642015dn94000413.

[11] Yevgeniya A. Abramzon et al. "The Overlapping Genetics of Amyotrophic Lateral Sclerosis and Frontotemporal Dementia". In: *Frontiers in Neuroscience* 14 (Feb. 2020). DOI: 10.3389/fnins.2020.00042. URL: https://doi.org/10.3389/fnins.2020.00042.

[12] Alexander E. Volk et al. "Current knowledge and recent insights into the genetic basis of amyotrophic lateral sclerosis". In: *medizinische genetik* 30.2 (June 2018), pp. 252–258. DOI: 10.1007/s11825-018-0185-3. URL: https://doi.org/10.1007/s11825-018-0185-3.

[13] Louise Benarroch et al. "The 2021 version of the gene table of neuromuscular disorders (nuclear genome)". In: *Neuromuscular Disorders* 30.12 (Dec. 2020), pp. 1008–1048. DOI: 10.1016/j.nmd.2020.11.009. URL: https://doi.org/10.1016/j.nmd.2020.11.009.

[14] Mirjana Babić Leko et al. "Molecular Mechanisms of Neurodegeneration Related to C9orf72 Hexanucleotide Repeat Expansion". In: *Behavioural Neurology* 2019 (Jan. 2019), pp. 1–18. DOI: 10.1155/2019/2909168. URL: https://doi.org/10.1155/2019/2909168.

[15] Sarat C. Vatsavayai et al. "Timing and significance of pathological features in *C9orf72* expansion-associated frontotemporal dementia". In: *Brain* 139.12 (Oct. 2016), pp. 3202–3216. DOI: 10.1093/brain/aww250. URL: https://doi.org/10.1093/brain/aww250.

[16] Jakub Scaber and Kevin Talbot. "What is the role of TDP-43 inC9orf72-related amyotrophic lateral sclerosis and frontemporal dementia?" In: *Brain* 139.12 (Dec. 2016), pp. 3057–3059. DOI: 10.1093/brain/aww264. URL: https://doi.org/10.1093/brain/aww264.

[17] Yeomin Yun and Yoon Ha. "CRISPR/Cas9-Mediated Gene Correction to Understand ALS". In: *International Journal of Molecular Sciences* 21.11 (May 2020), p. 3801. DOI: 10.3390/ijms21113801. URL: https://doi.org/10.3390/ijms21113801.

[18] Simran J. Kaur, Stephanie R. McKeown, and Shazia Rashid. "Mutant SOD1 mediated pathogenesis of Amyotrophic Lateral Sclerosis". In: *Gene* 577.2 (Feb. 2016), pp. 109–118. DOI: 10.1016/j.gene.2015.11.049. URL: https://doi.org/10.1016/j.gene.2015.11.049.

[19] Samer Abou Ezzi, Makoto Urushitani, and Jean-Pierre Julien. "Wild-type superoxide dismutase acquires binding and toxic properties of ALS-linked mutant forms through oxidation". In: *Journal of Neurochemistry* 102.1 (July 2007), pp. 170–178. DOI: 10.1111/j.1471-4159.2007.04531.x. URL: https://doi.org/10.1111/j.1471-4159.2007.04531.x.

[20] Emma L. Scotter, Han-Jou Chen, and Christopher E. Shaw. "TDP-43 Proteinopathy and ALS: Insights into Disease Mechanisms and Therapeutic Targets". In: *Neurotherapeutics* 12.2 (Feb. 2015), pp. 352–363. DOI: 10.1007/s13311-015-0338-x. URL: https://doi.org/10.1007/s13311-015-0338-x.

[21] Chung-ke Chang et al. "Molecular mechanism of oxidation-induced TDP-43 RRM1 aggregation and loss of function". In: *FEBS Letters* 587.6 (Feb. 2013), pp. 575–582. DOI: 10.1016/j.febslet.2013.01.038. URL: https://doi.org/10.1016/j.febslet.2013.01.038.

[22] Sevastyan O. Rabdano et al. "Onset of disorder and protein aggregation due to oxidation-induced intermolecular disulfide bonds: case study of RRM2 domain from TDP-43". In: *Scientific Reports* 7.1 (Sept. 2017). DOI: 10.1038/s41598-017-10574-w. URL: https://doi.org/10.1038/s41598-017-10574-w.

[23] Archana Prasad et al. "Molecular Mechanisms of TDP-43 Misfolding and Pathology in Amyotrophic Lateral Sclerosis". In: *Frontiers in Molecular Neuroscience* 12 (Feb. 2019). DOI: 10.3389/fnmol.2019.00025. URL: https://doi.org/10.3389/fnmol.2019.00025.

[24] Nicol Birsa, Matthew Peter Bentham, and Pietro Fratta. "Cytoplasmic functions of TDP-43 and FUS and their role in ALS". In: *Seminars in Cell & Developmental Biology* 99 (Mar. 2020), pp. 193–201. DOI: 10.1016/j.semcdb.2019.05.023. URL: https://doi.org/10.1016/j.semcdb.2019.05.023.

[25] Terry R. Suk and Maxime W. C. Rousseaux. "The role of TDP-43 mislocalization in amyotrophic lateral sclerosis". In: *Molecular Neurodegeneration* 15.1 (Aug. 2020). DOI: 10.1186/s13024-020-00397-1. URL: https://doi.org/10.1186/s13024-020-00397-1.

[26] Chunhui Huang, Sen Yan, and Zaijun Zhang. "Maintaining the balance of TDP-43, mitochondria, and autophagy: a promising therapeutic strategy for neurodegenerative diseases". In: *Translational Neurodegeneration* 9.1 (Oct. 2020). DOI: 10.1186/s40035-020-00219-w. URL: https://doi.org/10.1186/s40035-020-00219-w.

[27] Eva Maria Johanna de Boer et al. "TDP-43 proteinopathies: a new wave of neurodegenerative diseases". In: *Journal of Neurology, Neurosurgery & Psychiatry* 92.1 (Nov. 2020), pp. 86–95. DOI: 10.1136/jnnp-2020-322983. URL: https://doi.org/10.1136/jnnp-2020-322983.

[28] Manuela Neumann et al. "Ubiquitinated TDP-43 in Frontotemporal Lobar Degeneration and Amyotrophic Lateral Sclerosis". In: *Science* 314.5796 (Oct. 2006), pp. 130–133. DOI: 10.1126/science.1134108. URL: https://doi.org/10.1126/science.1134108.

[29] Ju Gao et al. "TDP-43 proteinopathy and mitochondrial abnormalities in neurodegeneration". In: *Molecular and Cellular Neuroscience* 100 (Oct. 2019), p. 103396. DOI: 10.1016/j.mcn.2019.103396. URL: https://doi.org/10.1016/j.mcn.2019.103396.

[30] Han-Jou Chen and Jacqueline C. Mitchell. "Mechanisms of TDP-43 Proteinopathy Onset and Propagation". In: *International Journal of Molecular Sciences* 22.11 (June 2021), p. 6004. DOI: 10.3390/ijms22116004. URL: https://doi.org/10.3390/ijms22116004.

[31] Yu-Sheng Fang et al. "Full-length TDP-43 forms toxic amyloid oligomers that are present in frontotemporal lobar dementia-TDP patients". In: *Nature Communications* 5.1 (Sept. 2014). DOI: 10.1038/ncomms5824. URL: https://doi.org/10.1038/ncomms5824.

[32] Daisy Sproviero et al. "Pathological Proteins Are Transported by Extracellular Vesicles of Sporadic Amyotrophic Lateral Sclerosis Patients". In: *Frontiers in Neuroscience* 12 (July 2018). DOI: 10.3389/fnins.2018.00487. URL: https://doi.org/10.3389/fnins.2018.00487.

[33] Eduard Willms et al. "Extracellular Vesicle Heterogeneity: Subpopulations, Isolation Techniques, and Diverse Functions in Cancer Progression". In: *Frontiers in Immunology* 9 (Apr. 2018). DOI: 10.3389/fimmu.2018.00738. URL: https://doi.org/10.3389/fimmu.2018.00738.

[34] Jacopo Meldolesi. "Exosomes and Ectosomes in Intercellular Communication". In: *Current Biology* 28.8 (Apr. 2018), R435–R444. DOI: 10.1016/j.cub.2018.01.059. URL: https://doi.org/10.1016/j.cub.2018.01.059.

[35] Sabha Asghar et al. "Exosomes in intercellular communication and implications for osteoarthritis". In: *Rheumatology* (Oct. 2019). DOI: 10.1093/rheumatology/kez462. URL: https://doi.org/10.1093/rheumatology/kez462.

[36] Graça Raposo and Willem Stoorvogel. "Extracellular vesicles: Exosomes, microvesicles, and friends". In: *Journal of Cell Biology* 200.4 (Feb. 2013), pp. 373–383. DOI: 10.1083/jcb.201211138. URL: https://doi.org/10.1083/jcb.201211138.

[37] Ramesh Kakarla et al. "Apoptotic cell-derived exosomes: messages from dying cells". In: *Experimental & Molecular Medicine* 52.1 (Jan. 2020), pp. 1–6. DOI: 10.1038/s12276-019-0362-8. URL: https://doi.org/10.1038/s12276-019-0362-8.

[38] Paul D. Robbins and Adrian E. Morelli. "Regulation of immune responses by extracellular vesicles". In: *Nature Reviews Immunology* 14.3 (Feb. 2014), pp. 195–208. DOI: 10.1038/nri3622. URL: https://doi.org/10.1038/nri3622.

[39] Don Armstrong and Derek E. Wildman. "Extracellular Vesicles and the Promise of Continuous Liquid Biopsies". In: *Journal of Pathology and Translational Medicine* 52.1 (Jan. 2018), pp. 1–8. DOI: 10.4132/jptm.2017.05.21. URL: https://doi.org/10.4132/jptm.2017.05.21.

[40] Stephanie Boukouris and Suresh Mathivanan. "Exosomes in bodily fluids are a highly stable resource of disease biomarkers". In: *PROTEOMICS - Clinical Applications* 9.3-4 (Mar. 2015), pp. 358–367. DOI: 10.1002/prca.201400114. URL: https://doi.org/10.1002/prca.201400114.

[41] Edward Pajarillo et al. "The role of astrocytic glutamate transporters GLT-1 and GLAST in neurological disorders: Potential targets for neurotherapeutics". In: *Neuropharmacology* 161 (Dec. 2019), p. 107559. DOI: 10.1016/j.neuropharm.2019.03.002. URL: https://doi.org/10.1016/j.neuropharm.2019.03.002.

[42] Maja Mustapic et al. "Plasma Extracellular Vesicles Enriched for Neuronal Origin: A Potential Window into Brain Pathologic Processes". In: *Frontiers in Neuroscience* 11 (May 2017). DOI: 10.3389/fnins.2017.00278. URL: https://doi.org/10.3389/fnins.2017.00278.

[43] Mathilde Mathieu et al. "Specificities of exosome versus small ectosome secretion revealed by live intracellular tracking of CD63 and CD9". In: *Nature Communications* 12.1 (July 2021). DOI: 10.1038/s41467-021-24384-2. URL: https://doi.org/10.1038/s41467-021-24384-2.

[44] Sandra Anne Banack, Rachael Anne Dunlop, and Paul Alan Cox. "An miRNA fingerprint using neural-enriched extracellular vesicles from blood plasma: towards a biomarker for amyotrophic lateral sclerosis/motor neuron disease". In: *Open Biology* 10.6 (June 2020), p. 200116. DOI: 10.1098/rsob.200116. URL: https://doi.org/10.1098/rsob.200116.

[45] Yong Chen et al. "Increased Interleukin-6 Levels in the Astrocyte-Derived Exosomes of Sporadic Amyotrophic Lateral Sclerosis Patients". In: *Frontiers in Neuroscience* 13 (June 2019). DOI: 10.3389/fnins.2019.00574. URL: https://doi.org/10.3389/fnins.2019.00574.

[46] Francesca Pregnolato et al. "Exosome microRNAs in Amyotrophic Lateral Sclerosis: A Pilot Study". In: *Biomolecules* 11.8 (Aug. 2021), p. 1220. DOI: 10.3390/biom11081220. URL: https://doi.org/10.3390/biom11081220.

[47] Alexander G. Thompson et al. "CSF extracellular vesicle proteomics demonstrates altered protein homeostasis in amyotrophic lateral sclerosis". In: *Clinical Proteomics* 17.1 (Aug. 2020). DOI: 10.1186/s12014-020-09294-7. URL: https://doi.org/10.1186/s12014-020-09294-7.

[48] Natasha Vassileff et al. "Revealing the Proteome of Motor Cortex Derived Extracellular Vesicles Isolated from Amyotrophic Lateral Sclerosis Human Postmortem Tissues". In: *Cells* 9.7 (July 2020), p. 1709. DOI: 10.3390/cells9071709. URL: https://doi.org/10.3390/cells9071709.

[49] Julia Yelick et al. "Elevated exosomal secretion of miR-124-3p from spinal neurons positively associates with disease severity in ALS". In: *Experimental Neurology* 333 (Nov. 2020), p. 113414. DOI: 10.1016/j.expneurol.2020.113414. URL: https://doi.org/10.1016/j.expneurol.2020.113414.

[50] Ana Rita Vaz et al. "Overexpression of miR-124 in Motor Neurons Plays a Key Role in ALS Pathological Processes". In: *International Journal of Molecular Sciences* 22.11 (June 2021), p. 6128. DOI: 10.3390/ijms22116128. URL: https://doi.org/10.3390/ijms22116128.

[51] Carolina Cunha et al. "Downregulated Glia Interplay and Increased miRNA-155 as Promising Markers to Track ALS at an Early Stage". In: *Molecular Neurobiology* (June 2017). DOI: 10.1007/s12035-017-0631-2. URL: https://doi.org/10.1007/s12035-017-0631-2.

[52] Vaz Vaz et al. "Targeting astrocyte and motor neuron specific miRNAs to prevent neuro-immune dysregulation in ALS". In: *Frontiers in Cellular Neuroscience* 13 (2019). DOI: 10.3389/conf.fncel.2019.01.00049. URL: https://doi.org/10.3389/conf.fncel.2019.01.00049.

[53] Dmitry Petrov et al. "ALS Clinical Trials Review: 20 Years of Failure. Are We Any Closer to Registering a New Treatment?" In: *Frontiers in Aging Neuroscience* 9 (Mar. 2017). DOI: 10.3389/fnagi.2017.00068. URL: https://doi.org/10.3389/fnagi.2017.00068.

[54] Abraham Acevedo-Arozena et al. "A comprehensive assessment of the SOD1G93A low-copy transgenic mouse, which models human amyotrophic lateral sclerosis". In: *Disease Models & Mechanisms* 4.5 (Sept. 2011), pp. 686–700. DOI: 10.1242/dmm.007237. URL: https://doi.org/10.1242/dmm.007237.

[55] Diana Posa et al. "Recapitulation of Pathological TDP-43 Features in Immortalized Lymphocytes from Sporadic ALS Patients". In: *Molecular Neurobiology* 56.4 (July 2018), pp. 2424–2432. DOI: 10.1007/s12035-018-1249-8. URL: https://doi.org/10.1007/s12035-018-1249-8.

[56] Katarina Stoklund Dittlau et al. "Human motor units in microfluidic devices are impaired by FUS mutations and improved by HDAC6 inhibition". In: *Stem Cell Reports* 16.9 (Sept. 2021), pp. 2213–2227. DOI: 10.1016/j.stemcr.2021.03.029. URL: https://doi.org/10.1016/j.stemcr.2021.03.029.

[57] Manuela Neumann et al. "Phosphorylation of S409/410 of TDP-43 is a consistent feature in all sporadic and familial forms of TDP-43 proteinopathies". In: *Acta Neuropathologica* 117.2 (Jan. 2009), pp. 137–149. DOI: 10.1007/s00401-008-0477-9. URL: https://doi.org/10.1007/s00401-008-0477-9.

[58] Fuyuki Kametani et al. "Identification of casein kinase-1 phosphorylation sites on TDP-43". In: *Biochemical and Biophysical Research Communications* 382.2 (May 2009), pp. 405–409. DOI: 10.1016/j.bbrc.2009.03.038. URL: https://doi.org/10.1016/j.bbrc.2009.03.038.

[59] Irene G. Salado et al. "Protein Kinase CK-1 Inhibitors As New Potential Drugs for Amyotrophic Lateral Sclerosis". In: *Journal of Medicinal Chemistry* 57.6 (Mar. 2014), pp. 2755–2772. DOI: 10.1021/jm500065f. URL: https://doi.org/10.1021/jm500065f.

[60] Carolina Alquezar et al. "Targeting TDP-43 phosphorylation by Casein Kinase-1δ inhibitors: a novel strategy for the treatment of frontotemporal dementia". In: *Molecular Neurodegeneration* 11.1 (Apr. 2016). DOI: 10.1186/s13024-016-0102-7. URL: https://doi.org/10.1186/s13024-016-0102-7.

[61] Mikhail Skliar and Vasiliy S. Chernyshev. "Imaging of Extracellular Vesicles by Atomic Force Microscopy". In: *Journal of Visualized Experiments* 151 (Sept. 2019). DOI: 10.3791/59254. URL: https://doi.org/10.3791/59254.

[62] Daan Vorselen et al. "Mechanical Characterization of Liposomes and Extracellular Vesicles, a Protocol". In: *Frontiers in Molecular Biosciences* 7 (July 2020). DOI: 10.3389/fmolb.2020.00139. URL: https://doi.org/10.3389/fmolb.2020.00139.

[63] Xue Qiu and Niko Hildebrandt. "Rapid and Multiplexed MicroRNA Diagnostic Assay Using Quantum Dot-Based Förster Resonance Energy Transfer". In: *ACS Nano* 9.8 (July 2015), pp. 8449–8457. DOI: 10.1021/acsnano.5b03364. URL: https://doi.org/10.1021/acsnano.5b03364.

[64] Loreto Martínez-González et al. "Motor neuron preservation and decrease of in vivo TDP-43 phosphorylation by protein CK-1δ kinase inhibitor treatment". In: *Scientific Reports* 10.1 (Mar. 2020). DOI: 10.1038/s41598-020-61265-y. URL: https://doi.org/10.1038/s41598-020-61265-y.